



Article

Adaptive Slicing Method for Hermite Non-Planar Tessellated Surfaces Models

Yang Chen ¹, Ruichao Lian ², Shikai Jing ^{1,*} and Jiangxin Fan ¹

- School of Mechanical Engineering, Beijing Institute of Technology, Beijing 100081, China; 3120205251@bit.edu.cn (Y.C.); fanjx0321@bit.edu.cn (J.F.)
- ² Instrumentation Technology and Economy Institute, Beijing 100032, China; lianruichao@bit.edu.cn
- * Correspondence: jingshikai@bit.edu.cn

Abstract: This paper presents an adaptive slicing method for Hermite non-planar tessellated surfaces models to improve the geometric accuracy of Rapid Prototyping (RP). Based on the bending characteristics of Hermite curved triangles, a slicing method for a complete Hermite surface model, including the grouping, the construction of the topological relationships, and the calculation of the intersection contours, was employed. The adaptive layering method considering the normal vector at the vertexes of the Hermite curved triangles was employed to grain the variable thickness of all layers of the Hermite surface model. The classical Stanford bunny model illustrates the significant improvement in the accuracy of the proposed method compared to the traditional method.

Keywords: rapid prototyping; surface model; model features; slicing method; adaptive layering

MSC: 51-08

1. Introduction

Rapid Prototyping (RP) or Layer Manufacturing (LM) refers to the fabrication of parts layer-by-layer. At present, RP has been widely used in the automobile and aerospace industries and other fields [1–4]. However, geometric dimensioning and tolerancing errors in the parts manufactured by RP is still widespread [5,6]. The conversion of the format of models [7] and slicing of the tessellated model [8] both introduce errors in RP at the algorithm level, which limits the wider application of this technology in engineering [9,10].

In model conversion, a commonly used method to decrease the approximation error of a planar triangle model is to constantly subdivide the triangular facets of the whole tessellated model, which is low in efficiency and leads to a significant amount of model data and therefore data redundancy [11]. Approximating CAD models with curved triangles can decrease the approximation error without changing the number of facets, which is more effective. Recently, some modified tessellation methods that use curved triangles have been proposed. Paul et al. [12] proposed a file format based on Steiner surfaces, but the construction of the Steiner surface requires a lot of information which is difficult to obtain. Santosh et al. [13] used an improved biquadratic Bezier curve to tessellate the CAD surface; however, numerical or optimization methods are necessary for solving the tessellation. The Hermite surface construction method proposed by Lian et al. [14] not only effectively reduces the error introduced by the model conversion but also has significant advantages in data acquisition, construction complexity, and surface splicing. However, limited by the lack of corresponding slicing methods, it is still unable to generate contours for manufacturing.

Among surface slicing methods, discrete intersection methods and tracking intersection methods are widely used because of their good applicability [15,16]. However, discrete intersection methods [17] have problems with the breakpoint and discontinuity in the intersection of the discrete approximated surfaces. Tracking intersection methods [18–21]



Citation: Chen, Y.; Lian, R.; Jing, S.; Fan, J. Adaptive Slicing Method for Hermite Non-Planar Tessellated Surfaces Models. *Mathematics* **2024**, *12*, 1753. https://doi.org/10.3390/ math12111753

Academic Editors: Nicolae Dumitru and Adrian Sorin Rosca

Received: 11 April 2024 Revised: 10 May 2024 Accepted: 15 May 2024 Published: 5 June 2024



Copyright: © 2024 by the authors. Licensee MDPI, Basel, Switzerland. This article is an open access article distributed under the terms and conditions of the Creative Commons Attribution (CC BY) license (https://creativecommons.org/licenses/by/4.0/).

are mostly based on the construction of ordinary differential equations, which can obtain more continuous intersection results and have strong universality. However, for the surface model, which is comprised of multiple relatively separated surfaces in AM, a connection method for the surfaces is lacking. As a consequence, a slicing method for the whole surface model that can connect all the curved facets is needed.

Adaptive layering overcomes the problem of the uniform layering method. Although the build time increases significantly, the accuracy requirement improves [22,23]. Among existing adaptive layering methods, some methods automatically adjust the layer thickness based on the area deviation ratio and the volume change rate of the adjacent layers. However, the reference area and the volume of each layer are constantly changing, resulting in a large amount of calculations and a low efficiency [24,25]. There are other methods that adjust the layer thickness by the minimum plane normal vector of the model or the chord height of the staircase effect. The whole algorithm process is linear and needs to be determined and adjusted by height, which causes a low efficiency [26]. The methods that classify the surface of the model based on the characteristics of the model to adjust the layer thickness cause a large number of ineffective calculations for the feature judgment of the model perpendicular to the processing direction [27–29]. Moreover, all the above adaptive slicing methods are based on the planar triangle model and ignore the characteristics of the surface model. Therefore, there is a need for an adaptive layering method for surface tessellated models to control the geometric accuracy, which compromises with the building time of the RP.

Based on the above analysis, this paper presents an adaptive slicing method for Hermite non-planar tessellated surfaces models. Aiming at the Hermite surface model construction based on an AMF (Additive Manufacturing File), a slicing method for the whole surface models was proposed. According to the bending characteristics of the surface triangles in a Hermite surface model, the grouping of the surface triangles, the construction of the ordered topological relationship, and the calculation of the intersection contours were employed to calculate the slice contours of the Hermite surface model. Then, an adaptive slicing method considering the characteristics of the normal vector at the vertices of the model's curved triangles was employed. The model of the curved triangles was partitioned. Then, according to the normal vector information of the Hermite triangle vertices in each partition, the local layer thickness was determined, and the non-uniform slice positions of the surface model was obtained. Finally, the classic Stanford bunny Hermite surface model was used to illustrate the accuracy improvement of the proposed method.

2. Hermite Surface Model

The steps in the RP progress, such as layering, slicing, path filling, and support generation, are based on the approximating model obtained by converting the original design model [7]. At present, the commonly used approximating model is the planar triangle model, which represents the outer contour shape of the model with a set of planar triangles. Therefore, building the approximating model with a Hermite surface can be simplified to building a set of Hermite surface triangles based on the originally used triangle mesh. The expression of the third-order Hermite surface triangles [14] can be defined as shown in Equation (1):

$$\mathbf{S}(u,v) = \mathbf{C}_{00} + \mathbf{C}_{10}u + \mathbf{C}_{01}v + \mathbf{C}_{20}u^2 + \mathbf{C}_{11}uv + \mathbf{C}_{02}v^2 + \mathbf{C}_{21}u^2v + \mathbf{C}_{12}uv^2 + \mathbf{C}_{30}u^3 + \mathbf{C}_{03}v^3, 0 \le v \le u \le 1$$
(1)

where (u, v) is the parameter value of the curved triangle and $C_{00}, C_{10}, \ldots, C_{03}$ is the function of the vertex of the triangle and the tangent vector of the vertex. The parameterized definition of the triangle is shown in Figure 1:

Mathematics **2024**, 12, 1753 3 of 20

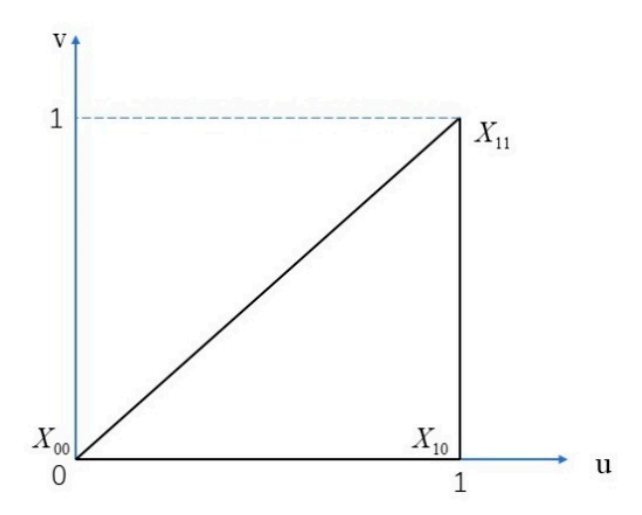


Figure 1. Parameter space of the Hermite triangle.

3. Slicing the Hermite Surface Model

3.1. Grouping of the Curved Triangles

The approximating model for the RP is usually composed of a large number of facets. The efficiency of the slicing algorithm can be greatly improved by grouping the facets that intersect the same slicing plane before calculating the contour of each layer. The Hermite surface model is different from the stereolithography (STL) model because of the bending characteristics of the Hermite surface triangles. The intersection between the model and the slicing plane can be divided into two cases, i.e., open and closed intersection lines, as shown in Figure 2a,b, respectively. When the intersecting line is a closed curve, the slicing plane does not intersect with any side of the curved triangle and Equation (2) is established, where **F** is an invariant force, T is a curved triangle, Z represents the slicing plane parallel to the XOY plane, L is the intersection line of T and Z, and $d\mathbf{s}$ is the directed curve element at L. Therefore, a new grouping method for models tessellated with Hermite curved triangles is needed. The grouping method proposed in this paper is shown in Figure 3.

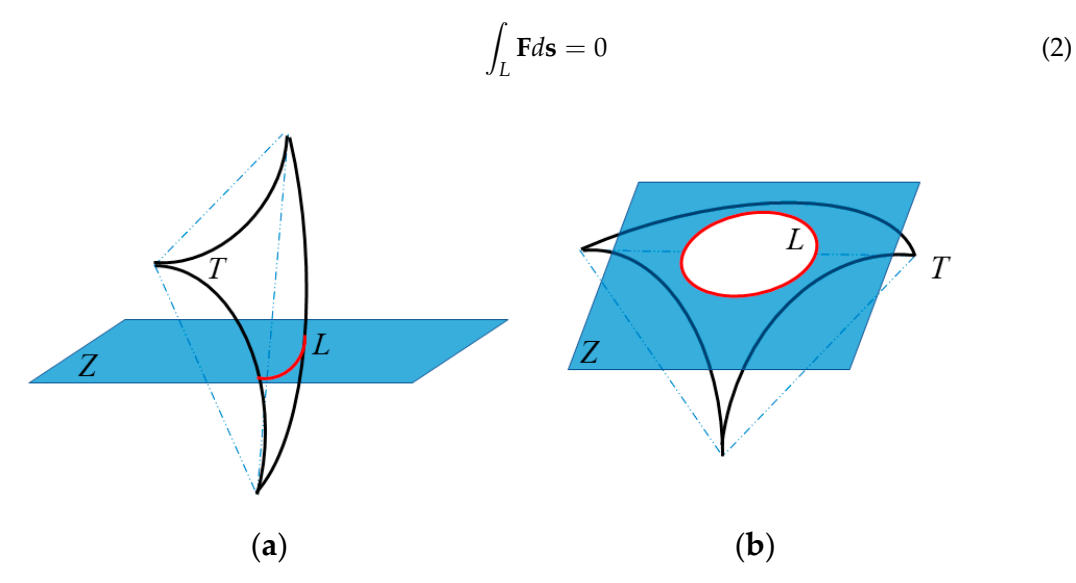


Figure 2. Hermite curved triangle: (a) open intersection, and (b) closed intersection.

Mathematics **2024**, 12, 1753 4 of 20

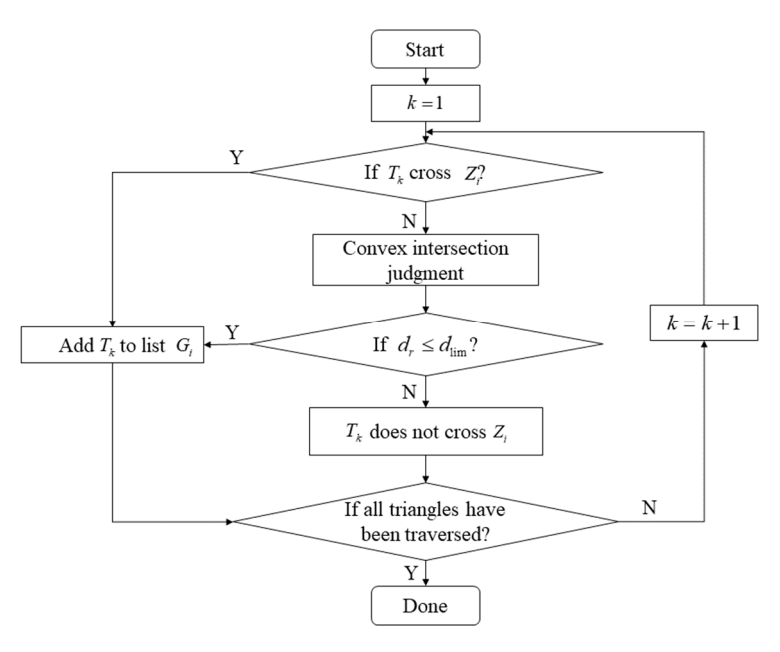


Figure 3. Grouping algorithm.

The cross-plane judgment method is shown in Equation (3), where z_{max} and z_{min} are the maximum and minimum values of the coordinates of the vertices and z_i is the z coordinate of the plane Z_i . If the triangle satisfies Equation (3), the triangle crosses the plane.

$$z_{\text{max}} \ge z_i, z_{\text{min}} \le z_i \tag{3}$$

A trend calculation method is adopted to judge whether the curved triangle intersects with the slicing plane, as shown in Figure 2b. This method uses the water droplets model [30] and transitions the problem into the problem of calculating the minimum distance between the curved triangle and the slicing plane. As shown in Figure 4, subject to the action of force \mathbf{D} , one point P above T carries out a slight motion on the tangent plane Π . The track curve of this motion can be written as $\mathbf{c}(s)$, where s is the arc length parameter. The drop follows the velocity \mathbf{C} defined by the orthogonal projection of \mathbf{D} onto the tangent plane Π , and it can be written as Equation (4):

$$\mathbf{C} = \frac{d\mathbf{c}}{ds} = \frac{\partial \mathbf{S}(u, v)}{\partial u} \frac{du}{ds} + \frac{\partial \mathbf{S}(u, v)}{\partial v} \frac{dv}{ds}$$
(4)

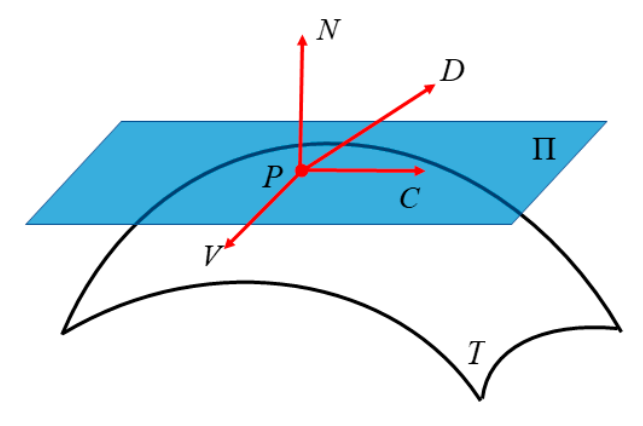


Figure 4. Water droplets method model.

If there is a vector $\mathbf{V}=\mathbf{D}\times\mathbf{N}$ in the tangent plane Π , then there is a relationship, as shown in Equation (5). Combining (5) with the first basic form of a surface (Equation (6)),

Mathematics **2024**, 12, 1753 5 of 20

the system of ordinary differential equations from the moving of point P on the surface T along the force \mathbf{D} is obtained, as shown in Equation (7).

$$\mathbf{c} \times \mathbf{V} = 0 \tag{5}$$

$$\mathbf{E}\left(\frac{du}{ds}\right)^{2} + 2\mathbf{F}\frac{du}{ds}\frac{dv}{ds} + \mathbf{G}\left(\frac{dv}{ds}\right)^{2} = 1$$
(6)

$$\frac{du}{ds} = \pm \frac{\mathbf{S}_v \cdot (\mathbf{D} \times \mathbf{N})}{\sqrt{\mathbf{E}(\mathbf{S}_v \cdot (\mathbf{D} \times \mathbf{N}))^2 - 2\mathbf{F}(\mathbf{S}_u \cdot (\mathbf{D} \times \mathbf{N}))(\mathbf{S}_v \cdot (\mathbf{D} \times \mathbf{N})) + \mathbf{G}(\mathbf{S}_u \cdot (\mathbf{D} \times \mathbf{N}))^2}}
\frac{dv}{ds} = \mp \frac{\mathbf{S}_u \cdot (\mathbf{D} \times \mathbf{N})}{\sqrt{\mathbf{E}(\mathbf{S}_v \cdot (\mathbf{D} \times \mathbf{N}))^2 - 2\mathbf{F}(\mathbf{S}_u \cdot (\mathbf{D} \times \mathbf{N}))(\mathbf{S}_v \cdot (\mathbf{D} \times \mathbf{N})) + \mathbf{G}(\mathbf{S}_u \cdot (\mathbf{D} \times \mathbf{N}))^2}}$$
(7)

where $\mathbf{E} = \mathbf{S}_u \cdot \mathbf{S}_u$, $\mathbf{F} = \mathbf{S}_u \cdot \mathbf{S}_v$, $\mathbf{G} = \mathbf{S}_v \cdot \mathbf{S}_v$, and $\mathbf{D}(x,y,z) = \nabla \mathbf{Z} = \pm [0,0,1]^T$. The fourth-order Runge–Kutta method is used to solve Equation (7). The qualified parameters are inserted into Equation (1) to obtain the coordinates of the nearest point with the slicing plane. Then the vertical distance d_r between the current iteration position and the slicing plane is calculated. If $d_r \leq d_{\lim}$, where d_{\lim} is the error threshold, there is an intersection line between the curved triangle and the slicing plane. Therefore, the triangle should be added to G_i , as shown in Figure 3.

3.2. Construction of the Sequential Topological Relationship

In order to obtain ordered model contour curves after slicing and to ensure the continuity and accuracy of the intersection data, it is necessary to determine the topological relationship of the triangles intersecting the slicing plane in the model. The intersection sequence of the curved triangles in a certain group usually presents as a closed loop, as shown in Figure 5a. However, due to the bending nature of the Hermite curved triangles, the topological adjacency of the curved triangles will appear as shown in Figure 5b. In this case, the number of times that the curved triangle appears in the topological relation table is not unique, which leads to the problem of the topological relation construction entering a dead corner and some curved triangles being omitted.

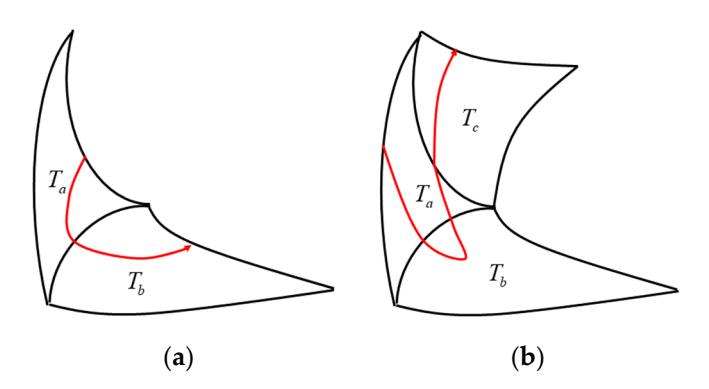


Figure 5. Adjacent relationship of triangles: (a) ideal topology case, and (b) topology error.

In the case where the topological relation enters a dead corner, if T_p is the reference triangle and $T_p = T_b$, then there is only one triangle satisfying Equation (8), which can be set as T_a . It can be entered into the topological relation table ${\bf R}$. Then, if $T_p = T_a$ and $T \notin {\bf R}$, which satisfies Equation (8), $T \neq T_b$ can be found. It can also be entered into the topological relation table ${\bf R}$. When the initial reference triangle is traversed, the topological relationship forms a complete closed loop and the topological relationship table is completed.

$$T_p \cap T = L, T \in G \text{ and } T \neq T_p$$
 (8)

When the topological relationship of the curved triangles is as shown in Figure 5b, the problem of missing a curved triangle may also occur, i.e., there is a $T \notin \mathbf{R}$, but $T \in G$. When $T_p = T_a$, there may be a T_c to satisfy Equation (8), but $T_c \cap T_p = P$. The result

Mathematics **2024**, 12, 1753 6 of 20

can be that the curved triangle T_b will not be judged in the judgement of the topological relationship between the subsequent edge connections. As a consequence, T_b is missed out. Therefore, it is necessary to build a topological chain for the missing curved triangles and to add it back to the corresponding position of the topological relation table. Only in this way can a complete topological relation table be constructed.

3.3. Calculation of the Intersection Contours

The intersection information between a model and the slicing plane in the AM process is an important basis for generating the final print path. Different from the STL and other plane triangle models, the intersection between the surface triangle and a plane is a curve. The method that only finds the intersection point between the surface triangle boundary and the slicing plane cannot determine the track of the intersection. Moreover, as shown in Figure 2b, when the intersection between the curved triangle and the slicing plane is a closed curve, the intersection line cannot be obtained by intersecting the surface boundary with the slicing plane. Therefore, a general method for calculating the intersection is proposed, which can obtain the intersection contours of the curved triangle and the slicing plane for various intersection situations. The intersection contour calculation algorithm is shown in Figure 6.

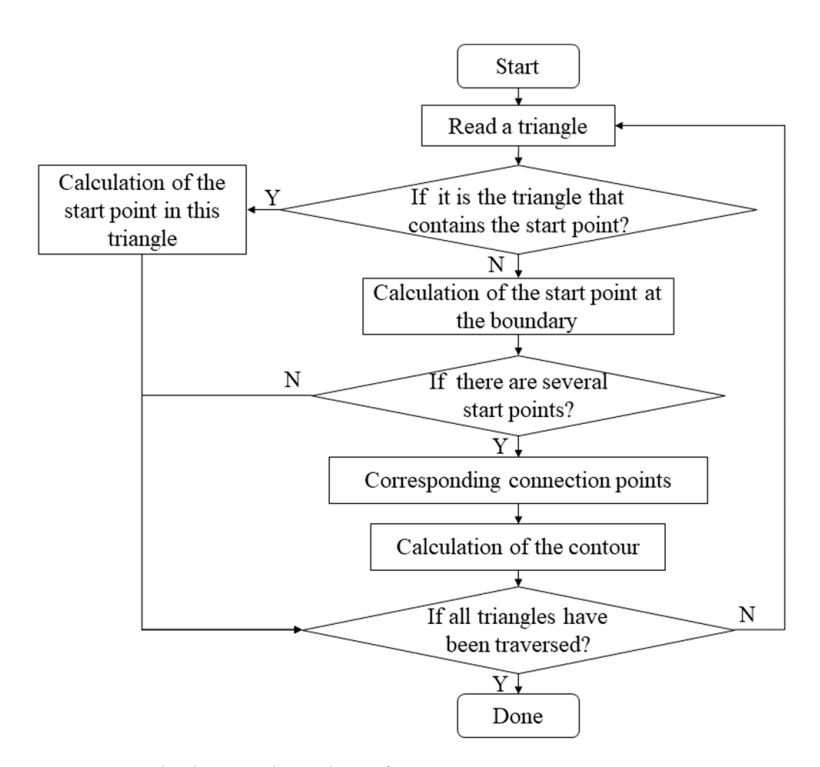


Figure 6. Calculation algorithm of intersection.

The starting point of the intersection line between the model and the slicing plane is calculated using the trend calculation model. As shown in Figure 7, $P_s(u_s, v_s)$ is the starting point of the intersection obtained by iterating forward on the surface, which can be either inside the Hermite curved triangle or on the extended surface of the curved triangle. Therefore, the parameter range is not restricted in the calculation of the intersection starting point. The calculated parameter values (u_s, v_s) can be substituted into Equation (1) to obtain the coordinate of the point, P(x,y), which is at the intersection between the triangle and the plane. Then d_r , which is the distance between P(x,y) and Z, can be calculated. When $d_r \leq d_{\lim}$, it can be supposed that the iterative position is located on the slicing plane and P(x,y) is the starting point of the desired intersection line.

Mathematics **2024**, 12, 1753 7 of 20

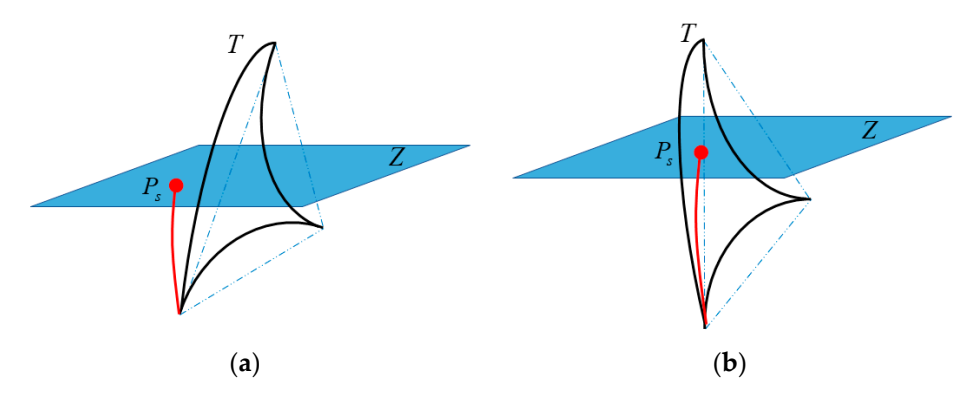


Figure 7. The starting point of the intersection line: (a) outside the triangle, and (b) inside the triangle.

The intersecting contour calculation is referred to in [31], and the intersection model of a curved triangle and slicing plane, as shown in Figure 8, is constructed. The velocity $\bf C$ is defined by the intersection of T and Z, and ${\bf c}(s)$ is the curve element in this direction, where s is the arc length parameter. If $\bf N_2$ is the normal vector of Z, then the equation $\bf C \times \bf N_2 = 0$ can be obtained. Combining it and Equation (4), Equation (9) can be obtained. Thus, the problem of solving the intersection contour of the curved triangle and the slicing plane is transformed into an orthogonal model. Finally, a system of two first-order ordinary differential equations, as shown in Equation (10), can be constructed by combining Equations (6) and (9). The initial condition is $u(0) = u_s$, $v(0) = v_s$ and the data point of the intersection between the first curved triangle in the group and the slicing plane can be obtained by solving Equation (10) with the Runge–Kutta method.

$$\frac{d\mathbf{c}}{ds} \cdot \mathbf{N}_2 = (\mathbf{S}_u \cdot \mathbf{N}_2) \frac{du}{ds} + (\mathbf{S}_v \cdot \mathbf{N}_2) \frac{dv}{ds} = 0$$
 (9)

$$\frac{du}{ds} = \pm \frac{\mathbf{S}_v \cdot \mathbf{N}_2}{\sqrt{\mathbf{E}(\mathbf{S}_v \cdot \mathbf{N}_2)^2 - 2\mathbf{F}(\mathbf{S}_u \cdot \mathbf{N}_2)(\mathbf{S}_v \cdot \mathbf{N}_2) + \mathbf{G}(\mathbf{S}_u \cdot \mathbf{N}_2)^2}}$$

$$\frac{dv}{ds} = \mp \frac{\mathbf{S}_u \cdot \mathbf{N}_2}{\sqrt{\mathbf{E}(\mathbf{S}_v \cdot \mathbf{N}_2)^2 - 2\mathbf{F}(\mathbf{S}_u \cdot \mathbf{N}_2)(\mathbf{S}_v \cdot \mathbf{N}_2) + \mathbf{G}(\mathbf{S}_u \cdot \mathbf{N}_2)^2}}$$
(10)

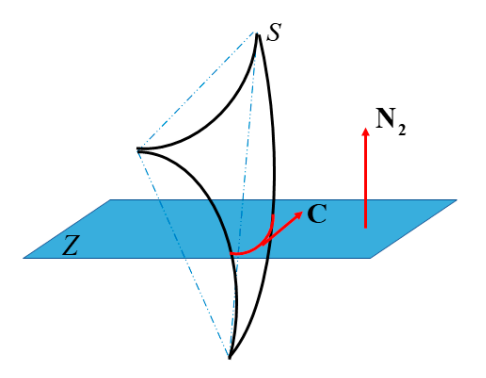


Figure 8. Intersection model.

In addition to the curved triangle where the starting point of the intersection line is located in the group, the other curved triangles need more complex calculations to obtain the initial value of the ordinary differential equation. Firstly, the adjacent edge of the curved triangles is searched and the boundary solving equation is constructed according to the parameter characteristics of the adjacent edge to obtain the parameters at the intersection point between the curved triangle boundary and the slicing plane. Taking the boundary curve $\mathbf{S}(u,0)$ as an example, the parameter value of the intersection point of the boundary curve and the slicing plane is as shown in Equation (11), where P_{sI} is the coordinates of the boundary intersection point. Given the height of the slicing plane, the parameter solving formula can be constructed as shown in Equation (12), where C_{00z} , C_{10z} , etc. represent the z

Mathematics **2024**, 12, 1753 8 of 20

component of C_{00} , C_{10} , etc. Then the parameter coordinates $p_{sI}(u_{sI}, 0)$ of the intersection point on the boundary curve can be obtained, which is the starting point of the intersection line between this curved triangle and the slicing plane.

$$\mathbf{S}(u,0) = \mathbf{C}_{00} + \mathbf{C}_{10}u + \mathbf{C}_{20}u^2 + \mathbf{C}_{30}u^3 = P_{sI}$$
(11)

$$\begin{cases} C_{00z} + C_{10z}u + C_{20z}u^2 + C_{30z}u^3 = z_{sI} \\ z_{sI} = z \end{cases}$$
 (12)

In the case that there is more than one intersection line on the same curved triangle, multiple intersection points will occur when the boundary curve intersects with the slicing plane, as shown in Figure 9. Therefore, it is necessary to calculate the distance between the coordinate position corresponding to multiple solutions and the end point of the intersection line. Then, the two points with the shortest distance should be connected.

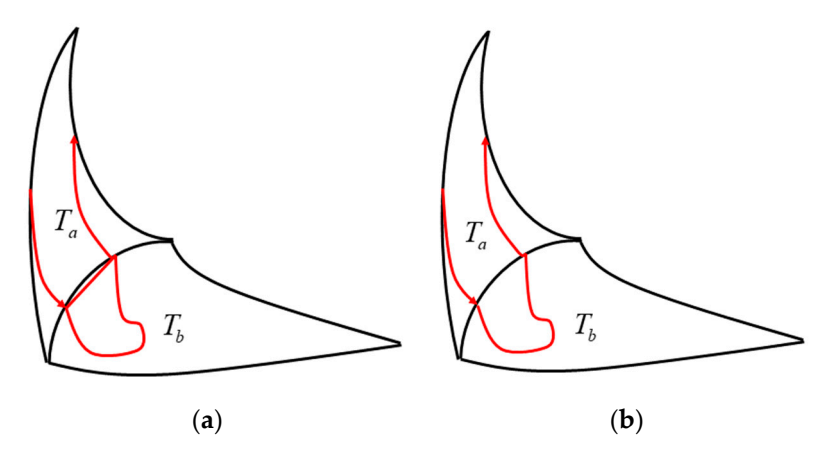


Figure 9. Case of multiple junctions: (a) correct connection, and (b) wrong connection.

4. Adaptive Layering of the Hermite Surface Model

4.1. Partitioning

Model partitioning can reduce the number of facets involved in the adaptive layer thickness calculation and improve the efficiency of the model processing. The curved triangles between two adjacent slicing planes or intersecting slicing planes are obtained by an equal thickness grouping method. First of all, it is judged whether the Hermite curved triangles are across the planes. If Equation (3) is met, the triangle crosses the planes, as shown in Figure 10d, and it should be stored in the corresponding equal thickness group. If the equation is not satisfied, there are three possibilities. If $z_i \leq z_{\text{max}} \leq z_{i+1}, z_i \leq z_{\text{min}} \leq z_{i+1}$, the position of the triangle is as shown in Figure 10c. If Equation (2) is met, it is as shown in Figure 10b. Otherwise, the curved triangle is located in the other layers (Figure 10a). Therefore, for the curved triangle that does not satisfy Equation (3), it should be further determined whether it is located between the two slicing planes according to the vertex coordinates and the convex intersection judgment method (which is the same as in Section 3.1).

After the equal thickness grouping of curved triangles is completed, the grouped curved triangles are initially partitioned according to the longitudinal section. The adjacent two longitudinal sections, \prod_i and \prod_{i+1} , are defined as Equation (13):

$$\begin{cases}
\prod_{i}: y = \tan\left(\frac{\pi(i-1)}{n}\right) \cdot \left(x - \frac{x_{\min} + x_{\max}}{2}\right) + \frac{y_{\min} + y_{\max}}{2} \\
\prod_{i+1}: y = \tan\left(\frac{\pi i}{n}\right) \cdot \left(x - \frac{x_{\min} + x_{\max}}{2}\right) + \frac{y_{\min} + y_{\max}}{2}
\end{cases}$$
(13)

First, the cross-longitudinal section is judged. Since the longitudinal section is perpendicular to the slicing plane, the coordinates in the Z direction can be ignored. Therefore, the problem of the position relationship between the curved triangle and the longitudinal

Mathematics **2024**, 12, 1753 9 of 20

section can be transformed into the two-dimensional position relationship between the vertex of the curved triangle and the line as shown in Figure 11.

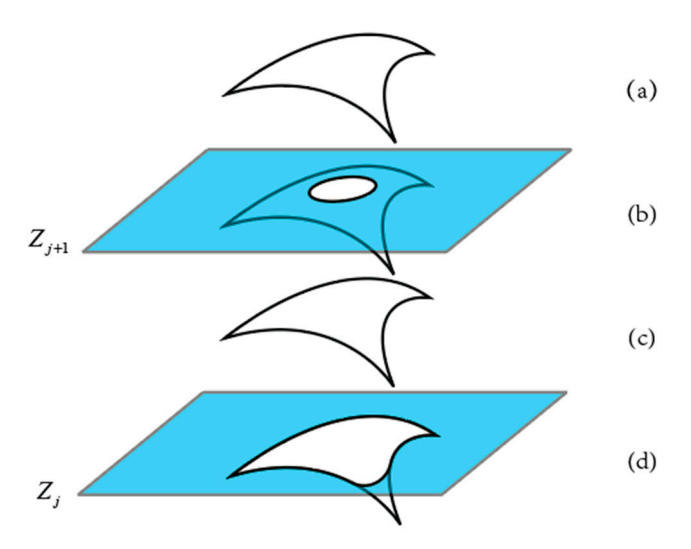


Figure 10. Grouping of curved triangles: (a) out of the two planes, (b) intersecting with one of the two planes and the intersection is a closed curve, (c) between the two planes, and (d) intersecting with one of the two planes and the intersection is an unclosed curve.

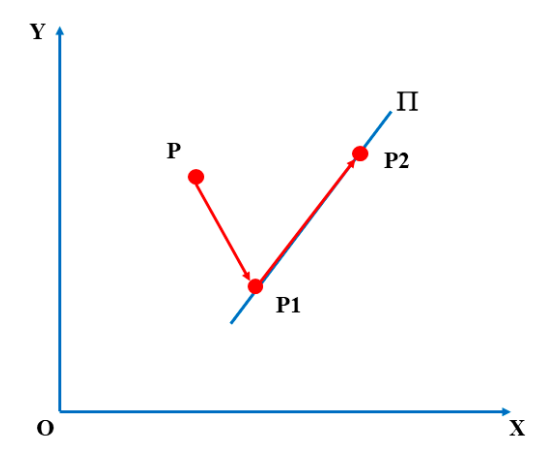


Figure 11. Position relationship between the curved triangle and the longitudinal section.

The point P in Figure 11 is the vertex of the curved triangles. P_1 and P_2 are two points on the longitudinal section. P_1P_2 is a directed line segment. The position judgment problem of point P and plane \prod_{P} is transformed into the problem of the position relationship between point P and vector P_1P_2 . The position judgment of P can be carried out by calculating the cross product of the vectors, as shown in Equation (14), to get the result of the cross product of the vectors, which can be written as S_P . When $S_P > 0$, P is on the left of P_1P_2 . When $S_P < 0$, P is on the right of P_1P_2 . When P_1P_2 is on the line of P_1P_2 . When all the three vertices of a curved triangle are not on the same side of the longitudinal slice, the curved triangle intersects the longitudinal section.

$$S_P = \overrightarrow{PP_1} \times \overrightarrow{P_1P_2} \tag{14}$$

The method of judging the intersection is used to judge whether the curved triangle is located in the partition between the two longitudinal sections \prod_i and \prod_{i+1} . It can also be accomplished by judging whether it is between the angle $\triangle \alpha_i$ formed by the two adjacent longitudinal sections. From point P to the two longitudinal sections \prod_i and \prod_{i+1} , a vertical

line is made, and the vertical feet are, respectively, P_i and P_{i+1} , as shown in Figure 12. When the point is located in the acute angle $\triangle \alpha_i$, the angle $\angle P_i P P_{i+1}$ is obtuse. Therefore, if $\angle P_i P P_{i+1}$ is obtuse, the vertex is located in the area of the angle $\triangle \alpha_i$ between the two longitudinal sections, and, if it is not obtuse, it is located in the area of the supplementary angle. When all the three vertices of a curved triangle are located in the region of $\triangle \alpha_i$, it can be considered that the curved triangle is located in the partition formed by the two longitudinal sections and belongs to the corresponding partition D_i .

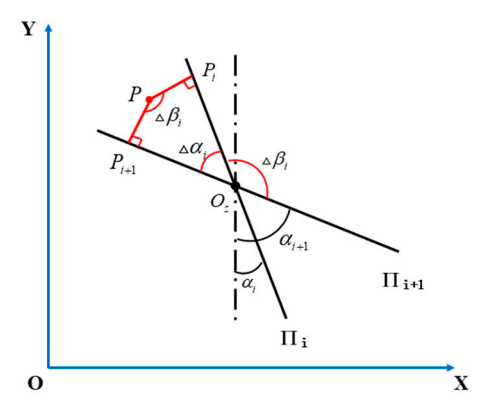


Figure 12. The method of intersection judgment.

However, as shown in Figure 13, due to the malleability of the plane in space, the preliminary partition result D_i of the curved triangle determined by the above method is essentially two subregions A and B of opposite angles, which needs to be further judged. A direction judgment method of the vertical point is proposed. The direction vector $\mathbf{d_i}$ and $\mathbf{d_{i+1}}$, after the normalization of the projection line of the two longitudinal sections, is calculated as Equation (15):

$$\begin{cases}
\mathbf{d_{i'}} = \left(1, \tan\left(\frac{\pi(i-1)}{n}\right), 0\right) \\
\mathbf{d_{i+1'}} = \left(1, \tan\left(\frac{\pi i}{n}\right), 0\right)
\end{cases}$$
(15)

Two vectors $\overrightarrow{P_iO_z}$ and $\overrightarrow{P_{i+1}O_z}$ that are perpendicular to the center of rotation are constructed, as shown in Figure 13. When their normalization results are the same as $\mathbf{d_i}$ and $\mathbf{d_{i+1}}$, the vertex P of the curved triangle can be considered to be located in region A; otherwise, P is located in region B.

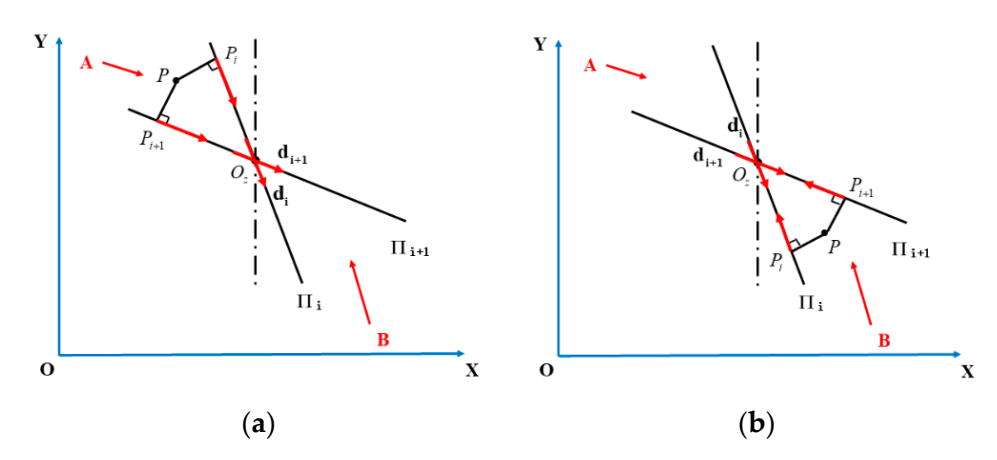


Figure 13. The position of the vertices of a curved triangle: (a) where the vertex is in zone A, and (b) where the vertex is in zone B.

4.2. Calculation of the Slicing Position

In AM, layering is needed to determine the thickness of each layer and the position of all slicing planes. The proposed adaptive layering method is based on the vertex normal vector of Hermite curved triangles, which can represent the characteristics of the curvature of the surface model. The vertex normal vector of a Hermite curved triangle is used to determine the local layer thickness that completely preserves the model features.

First, by traversing the partition D_{ip} , $p \in \{a, b\}$, the list P_{ip} , $p \in \{a, b\}$ of the vertices of the curved triangle with no repetition in the partition is obtained. According to the information of the curved triangle vertices in P_{ip} , the sum of the normal vectors of all vertices in the list \mathbf{N}_{ip}^a , including the maximum and minimum values in the list, which can be written as \mathbf{N}_{ip}^{\max} and \mathbf{N}_{ip}^{\min} , are, respectively, calculated as Equation (16), where $\mathbf{N}_{\mathbf{j}}$ represents the normal vector of the j th vertex.

$$\begin{cases}
\mathbf{N}_{ip}^{a} = \sum_{j=0}^{n} \mathbf{N_{j}} \\
\mathbf{N}_{ip}^{\max} = \max \left\{ \mathbf{N_{1}, N_{2}, \dots, N_{n}} \right\} \\
\mathbf{N}_{ip}^{\min} = \min \left\{ \mathbf{N_{1}, N_{2}, \dots, N_{n}} \right\}
\end{cases} (16)$$

Then, the base normal vector setting of partition D_{ip} is performed. The purpose of the proposed adaptive layering method is to reduce the staircase effect in model manufacturing and save manufacturing time. The staircase effect is caused by the surface mutation and the large angle between the model surface and the machining direction along the z axis. Therefore, the direction vector of the longitudinal section Π_i of the partition D_{ip} is set as the reference normal vector \mathbf{N}_{ip}^s , as shown in Equation (17). It can be taken as a comparison object of the normal vector within each group. In order to make the reference normal vector represent the most suitable surface conditions for processing, \mathbf{z}_{ip}^s is set to be zero.

$$\mathbf{N}_{ip}^{s} = \left[\cos(\alpha_i), \sin(\alpha_i), z_{ip}^{s}\right], i \in [1, n], p \in \{a, b\}$$
(17)

The angle between \mathbf{N}_{ip}^a and \mathbf{N}_{ip}^s can express the dip angle of the whole partition, which means it can be used to judge whether the partition needs to be manufactured with a small layer thickness. Since the proposed layering method only refers to the value of the normal vector in direction Z, the vector \mathbf{N}_{ip}^a is projected to the plane that passes the vector \mathbf{N}_{ip}^s and is perpendicular to the plane XOY, as shown in Figure 14. The projection vector $\widetilde{\mathbf{N}}_{ip}^a$ is represented as Equation (18):

$$\widetilde{\mathbf{N}}_{ip}^{a} = \mathbf{N}_{ip}^{a} - (\mathbf{N}_{ip}^{a} \times \mathbf{N}_{ip}^{f}) \mathbf{N}_{ip}^{f}$$
(18)

where $\mathbf{N}_{ip}^f = [-\sin(\alpha_i),\cos(\alpha_i),0]$ and θ_1^{ip} indicates the angle between \mathbf{N}_{ip}^s and $\mathbf{N}_{\mathbf{Aip}}^s$, as shown in Equation (19). In the same way, θ_{ip}^{\max} and θ_{ip}^{\min} , which indicate the angle between \mathbf{N}_{ip}^s and the projection normal of \mathbf{N}_{ip}^{\max} and \mathbf{N}_{ip}^{\min} , can be calculated.

$$\theta_{ip}^{a} = \arccos\left(\frac{\mathbf{N}_{ip}^{s} \cdot \widetilde{\mathbf{N}}_{ip}^{a}}{\left|\mathbf{N}_{ip}^{s}\right|\left|\widetilde{\mathbf{N}}_{ip}^{a}\right|}\right)$$
(19)

According to the rule of judging the angle, the characteristic normal vector in the partition is analyzed, and the initial judgment concerning whether the partition D_{ip} needs to be encrypted can be obtained. The angle threshold $-\frac{\pi}{2} \leq -\theta_{1st} \leq -\theta_{2st} \leq 0 \leq \theta_{2st} \leq \theta_{1st} \leq \frac{\pi}{2}$ is set to judge θ_{ip}^a . When it does not satisfy Equation (20), the overall slope of the surface of the partition is large and the whole partition needs to be encrypted.

$$-\theta_{1st} \le \theta_{in}^a \le \theta_{1st} \tag{20}$$

When θ_{ip}^a satisfies Equation (20), there may be four situations of this partition, as shown in Figure 15. Among them, there are two cases that need to be encrypted. The first one, as shown in Figure 15c, has a certain degree of inclination, but it is not enough to affect the angle of the partition. Secondly, as shown in Figure 15d, although there is a large degree of inclination, because of the positive and negative values in direction Z, there is a cancellation in the summation. For these four cases, θ_{ip}^{\max} and θ_{ip}^{\min} are used for further judgment.

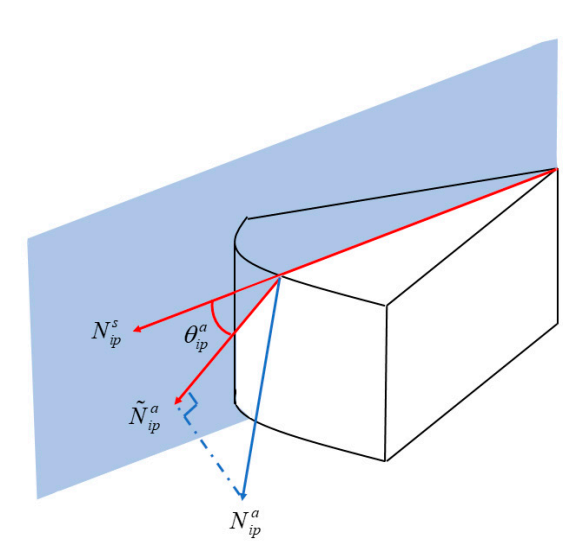


Figure 14. Setting of the reference normal vector.

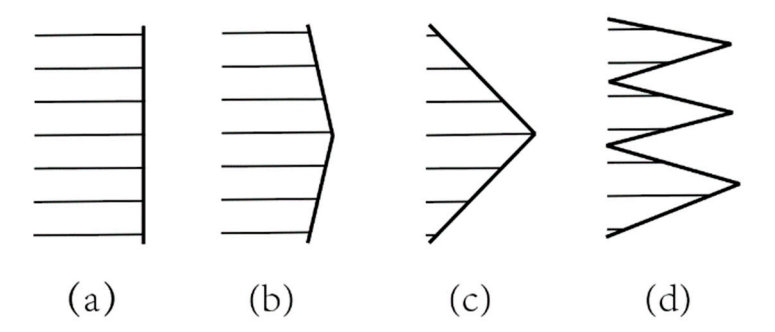


Figure 15. Sloping case of surface: (a) no slope, (b) no significant slope, (c) some slopes with a certain degree, and (d) slopes in the opposite direction.

When Equation (21) is satisfied and both θ_{ip}^{\min} and θ_{ip}^{\max} meet the gentle threshold θ_{2st} and $-\theta_{2st}$, it can be considered that the overall surface slope of the partition is not large, that is, the situation as shown in Figure 15b. Therefore, encryption of the layer thickness in this partition is not necessary.

$$-\theta_{2st} \le \theta_{ip}^{\min} \le \theta_{ip}^{\max} \le \theta_{2st} \tag{21}$$

When Equation (22) is not satisfied, there are large slope surfaces in the partition and there is a numerical offset, as shown in Figure 15d. Therefore, it is necessary to partially encrypt the partition.

$$-\theta_{1st} \le \theta_{ip}^{\min} \le \theta_{ip}^{\max} \le \theta_{1st} \tag{22}$$

When θ_{ip}^{max} and θ_{ip}^{min} satisfy Equation (22) but do not satisfy Equation (21), there are some faces with a large inclination in this partition, but the overall inclination of the

partition is not large, as shown in Figure 15c. In view of this situation, it is necessary to partially encrypt near the vertex that satisfies Equation (23) in this partition.

$$\theta_{ip} \in [-\theta_{1st}, -\theta_{2st}] \cup [\theta_{2st}, \theta_{1st}] \tag{23}$$

To determine the location of the model that requires encryption layering, the corresponding layer thickness needs to be calculated, as shown in Figure 16. In order to simplify the calculation, the common layer thickness calculation method of the STL model for adaptive layering is used for reference and the chord height h_s of the model is used to control the layer thickness.

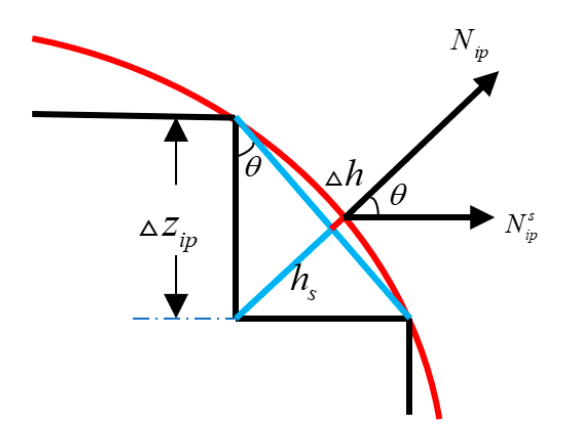


Figure 16. Layer thickness calculation.

After simplifying the surface to be a plane, the desired chord height h_s is set up, with the result that the layer thickness satisfies Equation (24).

$$\triangle z_{ip} = \frac{h_s}{\sin \theta} \tag{24}$$

If the surface is not simplified to be a plane, the chord height can be written as $(h_s + \triangle h)$. Due to the convexity of the surface triangle, there is $\triangle h \ge 0$. Then, the layer thickness can be written as Equation (25). Therefore, simplifying is better.

$$\Delta z_{ip}' = \frac{h_s + \Delta h}{\sin \theta} > \Delta z_{ip} \tag{25}$$

With the encryption judgment, the partitions of interval j between Z_j and Z_{j+1} are judged one by one, and the encryption condition of each partition D_{ji} is obtained. The table for the encryption condition in interval j that has n partitions can be obtained as Equation (26):

$$\mathbf{L}_{j} = \begin{bmatrix} \triangle z_{j}^{1}, Z_{\min}^{1}, Z_{\max}^{1} \\ \triangle z_{j}^{2}, Z_{\min}^{2}, Z_{\max}^{2} \\ \vdots \\ \triangle z_{i}^{n}, Z_{\min}^{n}, Z_{\max}^{n} \end{bmatrix}$$

$$(26)$$

where the first row of \mathbf{L}_j means that in the interval $[Z_{\min}^1, Z_{\max}^1]$ the layer thickness is $\triangle z_j^1$.

There is the condition, as shown in Equation (27), where there are intervals that have several $\triangle z_j$. Therefore, the layer thickness should be integrated. For the intervals J_f that have been evaluated and the interval $\left[Z_{\min}^p, Z_{\max}^p\right]$ that is being evaluated, integration occurs, as shown in Equation (28).

$$\left[Z_{\min}^{p}, Z_{\max}^{p}\right] \cap \left[Z_{\min}^{q}, Z_{\max}^{q}\right] \neq \emptyset, p, q \in [1, n] \text{ and } p \neq q$$
(27)

$$\left[Z_{trimin}^{p}, Z_{trimax}^{p}\right] - J_{f} = \left\{z \middle| z \in \left[Z_{\min}^{p}, Z_{\max}^{p}\right] \text{ and } z \notin J_{f}\right\}$$
(28)

Since encryption is aimed at better preserving the model features, for multiple encryption layer thicknesses corresponding to the same location interval, the smallest encryption layer thickness is preferred for the intervals, as shown in Equation (29) rather than Equation (27).

$$\triangle z_j^{p\prime} = \triangle z_j^{q\prime} = \min(\triangle z_j^p, \triangle z_j^q)$$
 (29)

The table of the preliminary result of the thickness of interval j could be written as shown in Equation (30).

$$\mathbf{J_e} = \begin{bmatrix} \triangle z_1 & z_{1\min} & z_{1\max} \\ \vdots & \vdots & \vdots \\ \triangle z_k & z_{k\min} & z_{k\max} \\ \vdots & \vdots & \vdots \\ \triangle z_n & z_{n\min} & z_{n\max} \end{bmatrix}$$
(30)

In RP, there is a limitation of the minimum layer thickness, which can be set as z_{lim} . The $\triangle z$ in $J_{\mathbf{e}}$ should be integrated as shown in Equations (31) and (32), where $z_{k+r\text{max}} - z_{k\text{min}} \ge z_{\text{lim}}$.

$$\triangle z = \min(\triangle z_k, \triangle z_{k+1}, \cdots, \triangle z_{k+r}) \tag{32}$$

The final table for encryption could be written as shown in Equation (33).

$$\mathbf{J} = \begin{bmatrix} \triangle z_1 & z_{1\min} & z_{1\max} \\ \vdots & \vdots & \vdots \\ \triangle z_p & z_{p\min} & z_{p\max} \\ \vdots & \vdots & \vdots \\ \triangle z_m & z_{m\min} & z_{m\max} \end{bmatrix}$$
(33)

For the pth interval $[z_{p\min}, z_{p\max}]$, a series of z coordinates of the slices can be obtained as $z_{p\min}$, $(z_{p\min} + \triangle z_p)$, $(z_{p\min} + 2 \triangle z_p)$, . . . , $z_{p\max}$. Therefore, after calculating all the intervals, the z coordinates of the slices for the whole model can be obtained as Equation (34).

$$z_{s} = \begin{bmatrix} z_{1\min}, (z_{1\min} + \triangle z_{1}), \cdots, z_{1\max} \\ \vdots \\ z_{p\min}, (z_{p\min} + \triangle z_{p}), \cdots, z_{p\max} \\ \vdots \\ z_{N\min}, (z_{N\min} + \triangle z_{N}), \cdots, z_{N\max} \end{bmatrix}$$

$$(34)$$

Finally, according to the slicing planes that are determined by Equation (34), the whole Hermite surface model could be achieved through adaptive layering.

5. Case Verification

In order to verify the feasibility and effectiveness of the proposed method, the Stanford bunny model, as shown in Figure 17, was selected for the case verification. The Stanford bunny model is a widely used 3D testing model in the field of computer graphics, produced at Stanford University in 1994, and is one of the classic graphics models. The Stanford bunny model can be downloaded from https://graphics.stanford.edu/data/3Dscanrep/ and accessed on 1 January 2023.

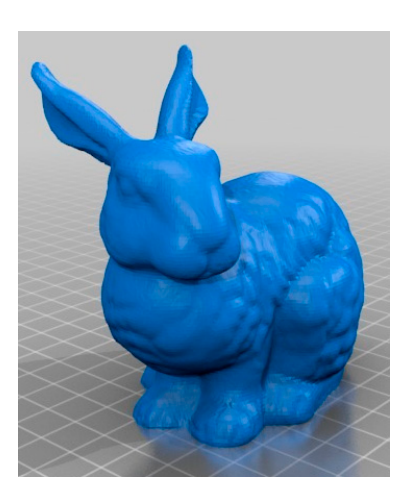


Figure 17. Stanford bunny.

The surface model obtained from the Stanford bunny solid design model used in this article consists of 165,528 surface triangles, including 82,766 vertices. The surface of the Stanford bunny model has many surface features, and there are multiple model contour features on the same horizontal plane, which can encompass the characteristics of general engineering models such as blades, camshafts, peristaltic robots inspired by inchworms [31], customized bone implants [32], etc. Compared to the models mentioned above, the Stanford bunny model has a higher surface complexity and a larger data volume, which can better test the algorithm proposed in this paper and ensure that it can be transferred to general engineering models.

Therefore, this paper takes the Stanford bunny model as an example for the method verification. Taking the Hermite surface model converted from the Stanford bunny solid model as the input, the AMF bunny model is sliced in equal thickness layers according to the Hermite surface model slicing method proposed in Section 3. The number of layers with an equal layer thickness is 14, and the corresponding slicing results are shown in Figure 18.

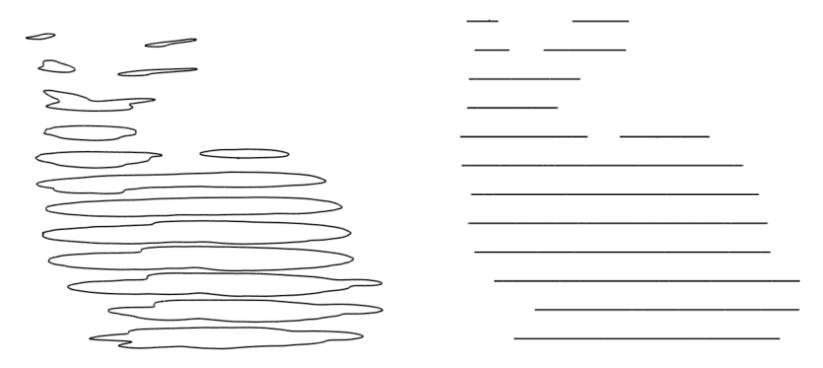


Figure 18. Equal layer thickness slicing results of the bunny model.

The model is sliced with the proposed Hermite surface model slicing method, and the section contour of each layer is obtained. This is compared with the slicing results of the STL model, which contains 391,696 planar triangles, and the fourth and ninth layers are shown in Figure 19. Where the blue area is the original model, the black line, the blue line, and the red line represent the original contour, the Hermite approximating contour, and the STL approximating contour, respectively. The degree of coincidence between the black line and the blue line or the red line represents the approximating accuracy. It is obvious that the blue line and the black line have a higher coincidence degree, which means that the proposed slicing method has a higher geometrical accuracy than the traditional STL slicing method.

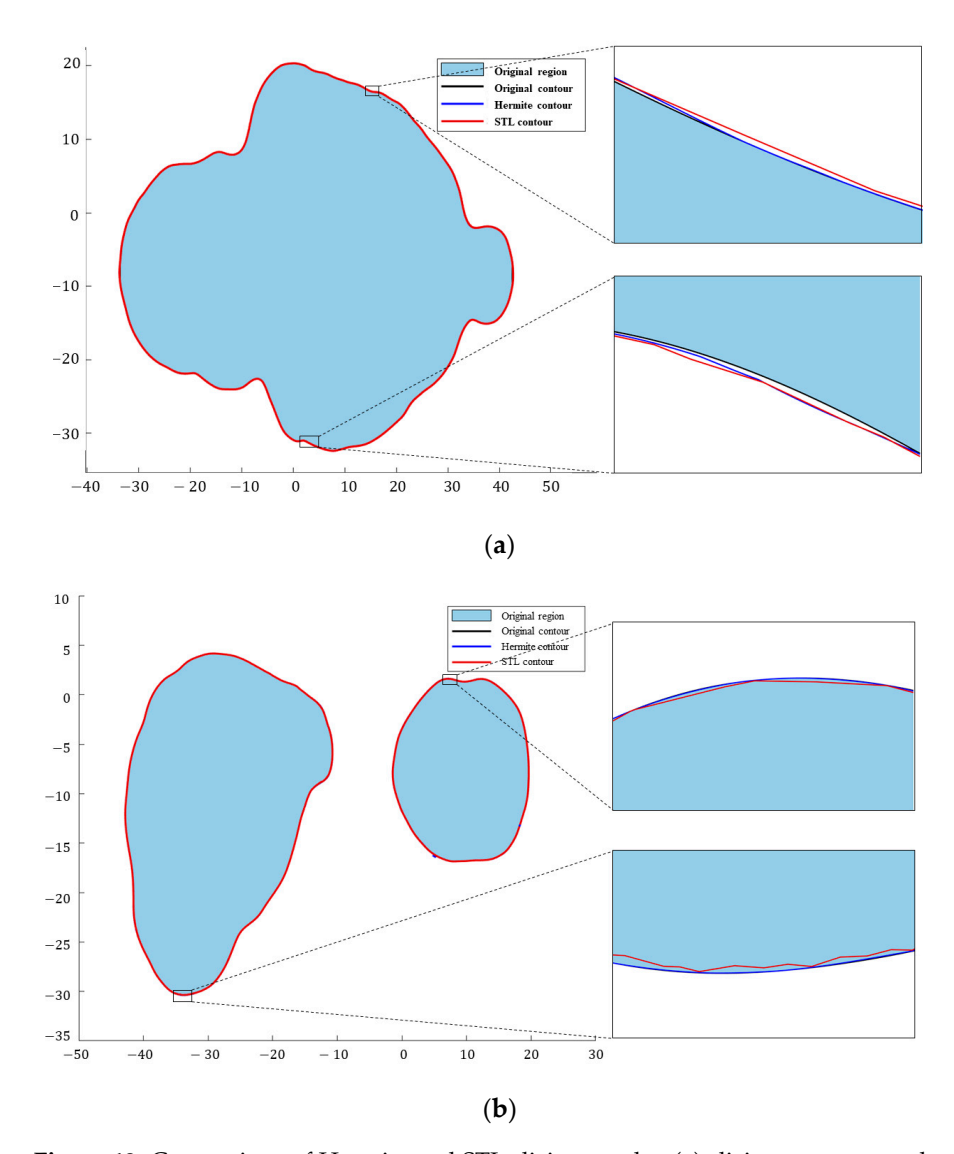


Figure 19. Comparison of Hermite and STL slicing results: (a) slicing contours at the fourth layer, and (b) slicing contours at the ninth layer.

In order to further evaluate the improvement of the geometrical accuracy in the proposed method, the original contours are extracted with the NX 12.0. The distance between the data point on the original contour and the slicing contour can measure the slicing error. Then, the slicing errors of the approximating contour of the Hermite model obtained by the proposed slicing method and the approximating contour of the STL model obtained by the conventional slicing method are calculated and compared, as shown in Table 1. Error calculation is not implemented on the first and last layers due to too few data points.

It can be observed from Table 1 that the average and maximum slice errors of the contours obtained from each layer of the Hermite surface model slicing are much lower than those of the STL model slicing. The average slicing error of each layer of the Hermite surface model is about 0.003, while the average slicing error of each layer of the STL plane model is about 0.05. The slicing error of the Hermite model is increased by 94.24%, compared with that of the STL plane model. The maximum error of each slice of the Hermite surface model is between 0.01 and 0.1, while the maximum error of each slice of the STL plane model is about 0.3. The maximum error of the Hermite model is usually one order of magnitude lower than that of the STL plane model. Figure 20 shows the variation in the mean error of all the layers generated by the two methods. The proposed slicing

method has a significantly lower and more stable error. It can be seen that the proposed slicing method significantly improves the slicing accuracy.

Table 1. Slicing errors and	error rates of the	approximation model.

No. of Layers	MAE of Hermite (mm)	MAE of STL (mm)	PCT of Lift (%)	MAX of Hermite (mm)	MAX of STL (mm)	PCT of Lift (%)
2	0.0031	0.0527	94.12	0.0154	0.2813	94.53
3	0.003	0.0504	94.05	0.0984	0.288	65.83
4	0.003	0.0575	94.78	0.018	0.3078	94.15
5	0.0029	0.0552	94.75	0.0173	0.3271	94.71
6	0.0029	0.0587	95.06	0.0156	0.3646	95.72
7	0.0028	0.0539	94.81	0.0102	0.3119	96.73
8	0.0031	0.0612	94.93	0.0156	0.3612	95.68
9	0.0033	0.0618	94.66	0.0358	0.3616	90.1
10	0.0032	0.0489	93.46	0.0185	0.2988	93.81
11	0.003	0.0552	94.57	0.0171	0.3079	94.45
12	0.0034	0.0547	93.78	0.0515	0.3962	87
13	0.0046	0.0565	91.86	0.0804	0.3948	79.64
Total	0.0032	0.0556	94.24	0.0328	0.3334	90.16

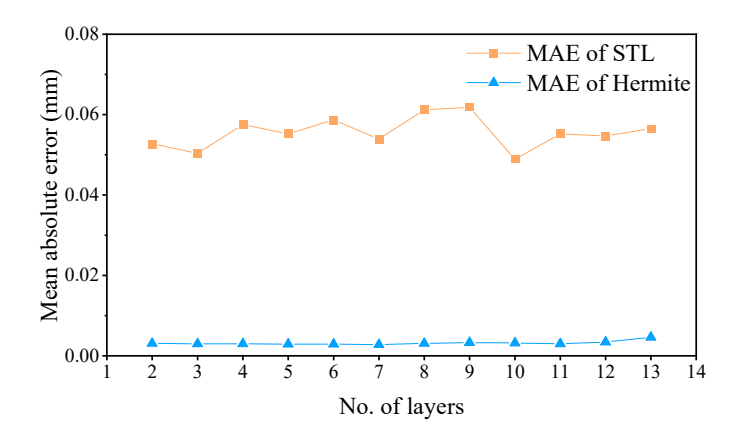


Figure 20. Variation in mean absolute error.

The proposed adaptive layering method of the Hermite surface model is used to perform adaptive layering on the bunny model. The number of layers is five, the number of longitudinal sections is three, $\theta_{1st} = \frac{\pi}{2}$, $\theta_{2st} = \frac{\pi}{6}$, and the chord height is set to be 1.5 mm. According to the characteristics of the model, the model is layered. The minimum layer thickness is set to 1.5 mm. Then, 51 slicing planes are obtained, and the layering results are shown in Figure 21a. The angle threshold is kept unchanged, the chord height is set to be 0.5 mm and the minimum layer thickness to be 0.5 mm, and, as a result, 141 non-uniformly distributed slicing planes are obtained, as shown in Figure 21b.

As shown in Figures 19 and 21, the layer thickness is significantly reduced in the areas with obvious features. The proposed adaptive layering algorithm can better identify the model features for the encryption layering, reduce the staircase effect, and improve the manufacturing accuracy of the additive manufacturing. As shown in Table 2, when the minimum layer thicknesses are the same, the error does not increase and the number of layers is reduced by 11.8% and 21.3%, respectively. Moreover, the smaller the minimum layer thickness is, the more obvious it is that the number of layers will be reduced. As can be seen from Figure 21a,b, different approximating accuracy requirements can be met by adjusting the chord height and the minimum layer thickness. Thus, the accuracy and manufacturing time can be well balanced.

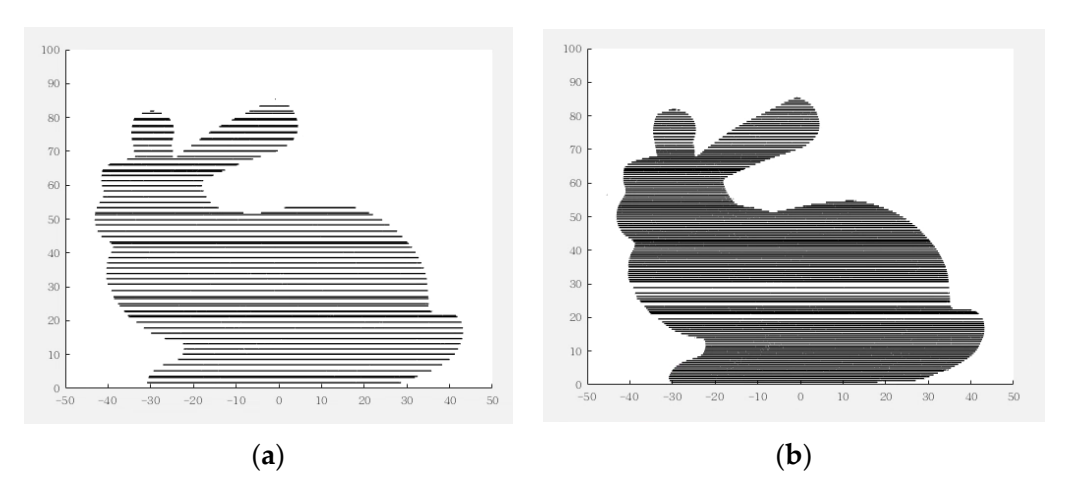


Figure 21. Results of adaptive layering of bunny model: (a) $h_s = 1.5$, $z_{lim} = 1.5$, and (b) $h_s = 0.5$, $z_{lim} = 0.5$.

Table 2. Comparison between the proposed method and the uniform layering method.

Method	Layer Height (mm)	Max Chord Error (mm)	No. of Layers
Uniform slicing	2	1.9971	43
Uniform slicing	1.5	1.499	57
Uniform slicing	0.5	0.5	171
Proposed method	1.5~2.0	1.5	51
Proposed method	0.5~1.5	0.5	141

6. Conclusions

Adaptive slicing for Hermite non-planar tessellated surfaces models was carried out based on an analysis of third-order Hermite surface triangles. For the Hermite surface model, considering the features of the surface triangles in the surface model, the surface model is sliced in order to ensure computational efficiency. Based on the surface characteristics of the Hermite surface model, the encryption layering interval and the adaptive layer thickness are calculated, the height set of the slicing plane is obtained, and the adaptive slicing of the surface model is implemented. The method handled the complex situation in the surface model and reduced the amount of data through preprocessing methods. It is proven that the slicing error of the proposed slicing method is reduced by an order of magnitude compared with the conventional STL slicing method on the classical Stanford bunny model. In addition, the proposed adaptive layering method significantly refines the feature region compared with the equal thickness slicing method and can satisfy the desire for geometrical accuracy while reducing the number of layers by about 10-20%. The proposed method is particularly suitable for objects with complex surfaces, for example, a peristaltic robot inspired by inchworms, customized bone implants, etc. Therefore, it has the potential to replace the existing adaptive slicing methods based on the planar approximation model, which are currently used in RP.

Author Contributions: Conceptualization, Y.C. and J.F.; methodology, Y.C. and J.F.; validation, S.J. and R.L.; investigation, J.F.; resources, Y.C. and J.F.; data curation, Y.C. and R.L.; writing—original draft preparation, Y.C. and J.F.; writing—review and editing, Y.C., R.L., and S.J.; visualization, R.L.; project administration, S.J.; and funding acquisition, S.J. All authors have read and agreed to the published version of the manuscript.

Funding: This work supported by the National Key R&D Program (Grant No.2023YFB4604800).

Data Availability Statement: The data will be made available by the authors on request.

Conflicts of Interest: The authors declare no conflict of interest.

References

1. Pham, D.T.; Gault, R.S. A comparison of rapid prototyping technologies. Int. J. Mach. Tools Manuf. 1998, 38, 1257–1287. [CrossRef]

- 2. Landers, R.; Hübner, U.; Schmelzeisen, R.; Mülhaupt, R. Rapid prototyping of scaffolds derived from thermoreversible hydrogels and tailored for applications in tissue engineering. *Biomaterials* **2002**, 23, 4437–4447. [CrossRef] [PubMed]
- 3. Blakey-Milner, B.; Gradl, P.; Snedden, G.; Brooks, M.; Pitot, J.; Lopez, E.; Leary, M.; Berto, F.; du Plessis, A. Metal additive manufacturing in aerospace: A review. *Mater. Des.* **2021**, 209, 110008. [CrossRef]
- 4. Aleisa, H.; Kontis, K.; Nikbay, M. Low Observable Uncrewed Aerial Vehicle Wind Tunnel Model Design, Manufacturing, and Aerodynamic Characterization. *Aerospace* 2024, 11, 216. [CrossRef]
- 5. Sachs, E.; Cima, M.; Cornie, J. Three-dimensional printing: Rapid tooling and prototypes directly from a CAD model. *CIRP Ann.* **1990**, 39, 201–204. [CrossRef]
- 6. Zhao, D.; Guo, W. Shape and performance controlled advanced design for additive manufacturing: A review of slicing and path planning. *Manuf. Sci. Eng.* **2019**, 142, 010801. [CrossRef]
- Zhu, Z.; Anwer, N.; Mathieu, L. Shape Transformation Perspective for Geometric Deviation Modeling in Additive Manufacturing. Procedia CIRP 2018, 75, 75–80. [CrossRef]
- 8. Gao, W.; Zhang, Y.; Ramanujan, D.; Ramani, K.; Chen, Y.; Williams, C.; Wang, C.; Shin, Y.; Zhang, S.; Zavattieri, D. The status challenges and future of additive manufacturing in engineering. *Comput. Aided Des.* **2015**, *69*, 65–89. [CrossRef]
- 9. Ngo, T.D.; Kashani, A.; Imbalzano, G.; Nguyen, K.T.; Hui, D. Additive manufacturing (3D printing): A review of materials, methods, applications and challenges. *Compos. Part B Eng.* **2018**, *143*, 172–196. [CrossRef]
- 10. Jafari, D.; Vaneker, T.H.J.; Gibson, I. Wire and arc additive manufacturing: Opportunities and challenges to control the quality and accuracy of manufactured parts. *Mater. Des.* **2021**, 202, 109471. [CrossRef]
- 11. Valentan, B.; Brajlih, T.; Drstvensek, I.; Balic, J. Basic solutions on shape complexity evaluation of STL data. *J. Achiev. Mater. Manuf. Eng.* **2008**, 23, 73–80.
- 12. Paul, R.; Anand, S. A new Steiner patch based file format for additive manufacturing processes. *Comput. Aided Des.* **2015**, *63*, 86–100. [CrossRef]
- 13. Allavarapu, S. A New Additive Manufacturing (AM) File Format Using Bezier Patches; University of Cincinnati: Cincinnati, OH, USA, 2013.
- 14. Lian, R.; Jing, S.; Chen, Y.; Fan, J. A Hermite Surface Triangle Modeling Method Considering High-Precision Fitting of 3D Printing Models. *Axioms* **2023**, *12*, 370. [CrossRef]
- 15. Boender, E. A survey of intersection algorithms for curved surfaces. Comput. Graph. 1991, 15, 109–115. [CrossRef]
- 16. Alsaidi RA, M.; Musleh, A. Two methods for surface/surface intersection problem comparative study. *Int. J. Comput. Appl.* **2014**, 92 1–8
- 17. Lee, R.B.; Fredricks, D.A. Intersection of parametric surfaces and a plane. IEEE Comput. Graph. Appl. 1984, 4, 48–51. [CrossRef]
- 18. Patrikalakis, N.M. Surface to surface intersections. Comput. Aided Des. Appl. 1993, 13, 1558–1756. [CrossRef]
- 19. Li, X.; Hong, J.; Song, C. An efficient surface-surface intersection algorithm based on geometry characteristics. *Comput. Graph.* **2004**, *28*, 527–537. [CrossRef]
- 20. Luo, R.C. Tracing Tangential surface-surface intersections. In Proceedings of the Third ACM Symposium on Solid Modeling and Applications, Salt Lake City, UT, USA, 17–19 May 1995; pp. 255–262.
- 21. Mukundan, H.; Ko, K.H.; Maekawa, T. Tracing surface intersections with validated ODE system solver. In *ACM Symposium on Solid and Physical Modeling, Proceedings of the Ninth ACM Symposium on Solid Modeling and Applications, Genoa, Italy, 9–11 June 2004*; Eurographics Association: Goslar, Germany, 2004; Volume 9, p. 9.
- 22. Mohan Pandey, P.; Venkata Reddy, N.; Dhande, S.G. Slicing procedures in layered manufacturing: A review. *Rapid Prototyp. J.* **2003**, *9*, 274–288. [CrossRef]
- 23. Dolenc, A.; Mäkelä, I. Slicing procedures for layered manufacturing techniques. Comput. Aided Des. 1994, 26, 119–126. [CrossRef]
- 24. Luo, N.; Wang, Q. Fast slicing orientation determining and optimizing algorithm for least volumetric error in rapid prototyping. *Int. J. Adv. Manuf. Technol.* **2016**, *83*, 1297–1313. [CrossRef]
- 25. Hu, J. Study on STL-based slicing process for 3D printing. In Proceedings of the 2017 International Solid Freeform Fabrication Symposium, Austin, TX, USA, 7–9 August 2017.
- 26. Taufik, M.; Jain, P.K. Surface roughness improvement using volumetric error control through adaptive slicing. *Int. J. Rapid Manuf.* **2017**, *6*, 279. [CrossRef]
- 27. Tata, K.; Fadel, G.; Bagchi, A.; Aziz, N. Efficient slicing for layered manufacturing. Rapid Prototyp. J. 1998, 4, 151–167. [CrossRef]
- 28. Ding, D.; Pan, Z.; Cuiuri, D.; Li, H.; Larkin, N.; Van Duin, S. Automatic multi-direction slicing algorithms for wire based additive manufacturing. *Robot. Comput. Integr. Manuf.* **2016**, *37*, 139–150. [CrossRef]
- 29. Wang, C.X.; Wang, Y.; Hao, Z.B. Segmentation adaptive slicing algorithm based on features of parts in additive manufacturing. *Chin. J. Eng. Des.* **2020**, *27*, 373–379.
- 30. Iglesias, A.; Puig, P.J.; Gálvez, A. Generating drop trajectories on parametric surfaces. CAD Graph. 2001, 1, 351–359.

31. Peng, Y.; Nabae, H.; Funabora, Y.; Suzumori, K. Controlling a peristaltic robot inspired by inchworms. *Biomim. Intell. Robot.* **2024**, 4, 100146. [CrossRef]

32. Meng, M.; Wang, J.; Huang, H.; Liu, X.; Zhang, J.; Li, Z. 3D printing metal implants in orthopedic surgery: Methods, applications and future prospects. *J. Orthop. Transl.* **2023**, 42, 94–112. [CrossRef]

Disclaimer/Publisher's Note: The statements, opinions and data contained in all publications are solely those of the individual author(s) and contributor(s) and not of MDPI and/or the editor(s). MDPI and/or the editor(s) disclaim responsibility for any injury to people or property resulting from any ideas, methods, instructions or products referred to in the content.